

# 4

## FUNCTIONAL MAPPING IN THE CAT PRIMARY VISUAL CORTEX USING HIGH MAGNETIC FIELDS

DAE-SHIK KIM, TIMOTHY Q. DUONG,  
KAMIL UGURBIL, AND SEONG-GI KIM

*Center for Magnetic Resonance Research University  
of Minnesota Medical School, Minneapolis, Minnesota*

### INTRODUCTION

In the mammalian brain cytoarchitectonically distinct areas form the basis for functional specialization (1). Such parcellation of the cortical tissue into functional subunits is especially prominent in the primary visual cortex of cats. Here, neurons with similar response properties, such as ocular dominance (2, 3), orientation (4, 5), and direction (6, 7) preferences, are clustered into "columns," spanning the entire cortical plate from the pia to the white matter.

Since the pioneering works of Hubel and Wiesel (2), the temporal and spatial properties of cortical columns in cat primary visual cortex have been studied extensively using a variety of techniques. Understanding of the temporal properties of the cortical columns promises to reveal the "neural code" of the brain's information processing, and elucidation of its spatial properties will shed light on how such codes are physically implemented across the cortex.

To this end, however, the applicability and fidelity of the traditional techniques to achieve this goal differ markedly. The use of single and multiunit recordings provides a good tool for assessing the temporal properties of cortical columns; finding a technique that can yield the spatial properties of cortical columns with

comparable accuracy, convenience, and applicability proved to be a much more difficult task.

In this chapter, we describe recent advances in functional magnetic resonance imaging (fMRI) we have made that will enable the functional organization of the cat visual cortex to be studied at "columnar" level, thereby approximating the spatial resolution of multielectrode and optical imaging techniques, but without their limitations. These advances should lay the foundation for future noninvasive exploration of animal and human brains at the fundamental level of its columnar architecture noninvasively. In ~~Chapter 5~~, we describe the imaging principles and techniques of this new method and present the first MRI studies of the functional activity in cat primary visual cortex at columnar resolution (see also Kim et al. [8]).

Chapter 4

#### LIMITATIONS OF CURRENT TECHNIQUES, OR WHY WE NEED ANOTHER MAPPING TECHNIQUE

The spatial layout of the functional architecture in cat primary visual cortex has been studied extensively using a variety of different techniques (see LeVay and Nelson [9] and Chapter 1 for review). Although these techniques have provided pivotal insights, each of the traditional mapping techniques suffers from a fundamental limitation. For example, the multielectrode mapping method lacks sufficient field of view and spatial resolution (7), ~~but~~ the 2-deoxyglucose method is not viable for in vivo mapping (10). The more recently developed "optical imaging of intrinsic signals" allows the simultaneous recording of neuronal activity over large areas of cortex (11,12). For example, in cat primary visual cortex, this technique has been utilized extensively to examine the tangential organization of multiple cortical maps and their topological relationships to each other at a columnar resolution 13, 14) (see Chapter 2). However, optical imaging at this spatial resolution is an invasive technique, because a craniotomy has to be made to expose the cortical surface. Furthermore, the applicability of optical imaging is limited to the superficial layers of the cortical surface only (15-17), thus failing to reveal activation signals originating from deeper cortical layers or from subcortical structures.

while

#### FUNCTIONAL MAGNETIC RESONANCE IMAGING

To further facilitate our understanding of the cortical information processing in adult and developing animals, it is imperative to devise a novel method that can visualize the functional architecture of the living brain without the aforementioned limitations. The rapid progress of blood oxygenation level-dependent (BOLD) functional magnetic resonance imaging (fMRI) in recent years has

raised the hope that this could be achieved. Using the paramagnetic deoxyhemoglobin as an endogenous contrast agent (18, 19), BOLD-based functional images can be obtained in vivo (in contrast to the 2-deoxyglucose technique) without the use of extrinsic contrast agents (in contrast to the positron emission technique), and from the entire brain (in contrast to the optical imaging of intrinsic signals). Most importantly, the noninvasiveness of MRI suits it well for studying the functional architecture of both the human and animal brains, thus enabling direct comparisons of putative homolog functions between humans and animals.

Despite these advantages, crucial questions must be answered before functional MRI can be utilized for addressing neurophysiological questions. For example, numerous BOLD studies during cognitive (20), motor (21), and perceptual (22–25) tasks indicate a good spatial correlation between neuronal and hemodynamic responses at a scale of several millimeters to centimeters. With this coarse scale, however, it is impossible to discriminate between the cortical columns representing individual receptive field properties, as the average periodicity between two adjacent isofunctional columns is about 1mm in most mammalian species (26). Furthermore, the ultimate functional specificity of fMRI remains highly controversial because the BOLD signal represents a complex convolution of metabolic and hemodynamic processes that is poorly understood (27).

Recent results from our laboratory and other laboratories now suggest that there is an intriguing relationship between the details of cortical hemodynamic responses and the ultimate spatial resolution of functional MRI. If utilized properly, this information will enable us to improve the functional specificity of fMRI far beyond what is achievable today.

#### Nuclear Magnetic Resonance and Magnetic Resonance Imaging

As the majority of the readers of this volume may not have a firsthand experience with high-field fMRI, it is worthwhile to start our discussion with a brief description of the theoretical and technical foundations of fMRI.

The phenomenon of nuclear magnetic resonance (NMR) was described in landmark articles more than 50 years ago (28, 29). The proton nucleus of the hydrogen atom, which is used for most imaging studies, possesses a small magnetic moment. When placed in a strong and homogenous magnetic field (“static field”,  $B_0$ ), the atoms align themselves with this field and reach a thermal equilibrium. The nuclei precess about the static field at a characteristic frequency (Larmor frequency), but at a random orientation with respect to each other. Application of a brief radio frequency excitation pulse (RF pulse) with Larmor frequency induces a rotating magnetic field orthogonal to the static field, thus causing the nuclei to precess away from the equilibrium. Using a “receiver coil,” the resulting rotating magnetic moment of the combined nuclei can then be observed as a time-dependent electromagnetic signal. Three of the parameters that can be observed in NMR are (1) the longitudinal relaxation time constant (“spin-lattice relaxation”);  $T_1$ , is the constant that characterizes the nuclei reapproaching the thermal

$T_2^*$  within and surrounding the vessels, which in turn results in *decreases* in the transverse relaxation times ( $T_2$  and  $T_2^*$ ) (18, 36). During the activation of the brain, this process is reduced: an increase in neuronal and metabolic activity results in a *reduction* of the relative deoxyhemoglobin concentration owing to an increase of blood flow (and hence increased supply of fresh oxyhemoglobin) that follows. Consequently, in conventional BOLD fMRI, brain "activity" can be measured as an *increase* in  $T_2$  or  $T_2^*$  weighted MR signals (19, 33, 34).

Vasculature Issues

BOLD fMRI is founded on the pioneering discovery of Roy and Sherrington (37), that changes in electrical activity are coupled to hemodynamic responses in the vasculature system. Consequently, for a proper understanding of the BOLD signals, the size, geometry, and location of the cortical vasculature surrounding the neural tissue must be considered. For the sake of further discussion, we define a microvascular/tissue component as an area of rapid exchange between blood water and tissue water (i.e., capillaries and adjacent tissues). In the parenchymal tissue of the cat cerebral cortex, such capillaries form a dense network with an average spacing of about 20  $\mu\text{m}$  (38). By contrast, the macrovascular component is composed of arteries, small arterioles, small venules, and veins, where such an exchange does not exist.

It is well known that, with typical fMRI acquisition parameters, the BOLD response is particularly sensitive in and around large "draining veins," which are usually distant from the sites of elevated neuronal activity (27, 39, 40). Thus it is reasonable to assume that conventional BOLD-based fMRI may overrepresent the "non-functional" large-vessel contribution, whereas the functional signals from small capillaries may be masked. Furthermore, recent optical spectroscopy data (41, 42) also suggest that there is an intimate relationship between the source of the hemodynamic signal and its spatial specificity. In particular, signals from large draining vessels were found to be spread out up to 3 to 7 mm from the actual site of electrical activity (43).

In any kind of brain mapping method based on hemodynamic activity, it is imperative to minimize the perturbative effect of draining vessels. To this end, our attempt to visualize cortical columns with functional MRI is aided by the fact that the vascular origin of the BOLD effect depends heavily on *magnetic field strength*. BOLD response is expected to behave according to the following equations (27, 44):

$$R_2^* = \alpha \{ \Delta\chi_0 \omega_0 (1-Y) \} b_{vl} \quad (\text{large blood vessels}) \quad (1)$$

$$R_2^* = \eta \{ \Delta\chi_0 \omega_0 (1-Y) \}^2 b_{vsP} \quad (\text{small blood vessels}) \quad (2)$$

where  $R_2^* = 1/T_2^*$ ,  $\alpha$  and  $\eta$  are constants,  $\omega_0$  is the external magnetic field in frequency units (rad/sec),  $\Delta\chi_0$  is the maximum susceptibility difference expected in the presence of fully deoxygenated blood,  $Y$  is the fraction of oxygenated blood

therefore  $\rightarrow \Delta\chi_0$

$$\rightarrow R_2^* = \eta \{ \Delta\chi_0 \omega_0 (1-Y) \}^2 b_{vsP}$$

space

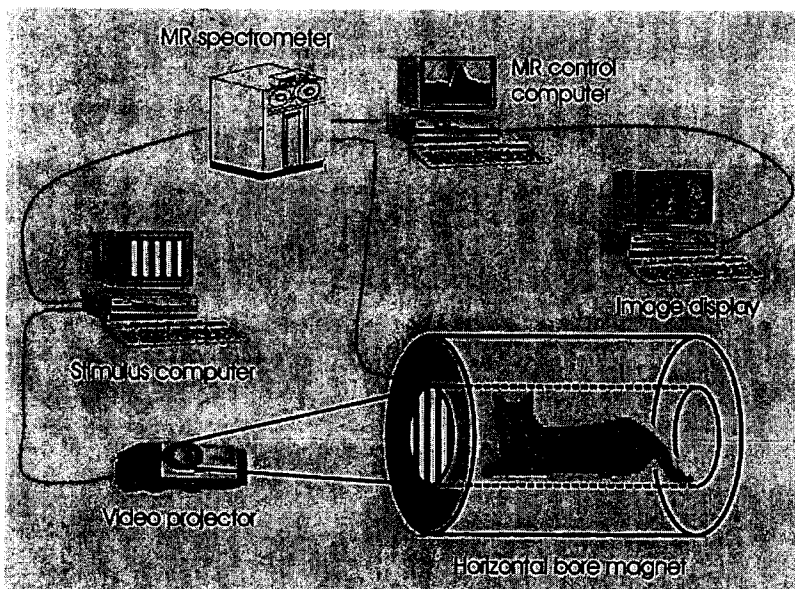


FIGURE 4-1. High-field cat MR experimental setup. Anesthetized cat was placed in a custom designed, MR-compatible stereotaxic holder and inserted into the isocenter of a 4.7 or 9.4 Tesla horizontal bore magnet. A video projector was used to stimulate the animal with moving gratings of four different orientations. Stimulus presentation was synchronized with MR data acquisition. See text for details.

( 135°) optimized to ~~strongly~~ activate neurons in cat area 18 (48). We have used area 18 for our studies because the distance between two iso-orientation columns in this area is wider than in area 17, thus maximizing our chance of resolving individual columns. Furthermore, the cat area 18 on the ~~marginal~~ *marginal* gyrus is essentially flat and can be covered by a single imaging slice. Area 17 is curved around the occipital pole and causes more susceptibility artifacts in MR images.

A small surface coil, 1.2 cm in diameter, was placed on top of the animal's head corresponding to the Horsley-Clark A3. All MR experiments were performed on a 4.7-T/40 cm (Oxford, UK) or 9.4-T/31 cm (Magnex, UK) horizontal MRI scanners equipped with a 15-G/cm or 30-G/cm magnetic field gradients, respectively. Figure 4-2 shows mid-sagittal (Fig. 4-2A), coronal (Fig. 4-2B), and axial (Fig. 4-2C) anatomical images of the cat brain obtained with a 9.4 Tesla magnet. The *sulcus cruciatus*, *sulcus splenialis*, and *sulcus suprasplenialis* are readily detectable on the mid-sagittal image. The white and gray matters in coronal and axial images are visible as bright and dark areas, respectively. Panel d displays the surface image of the left and right lateral gyri (left and right half of the image). The center of this surface image was at the anteroposterior 3 of the Horsley-Clark coordinate system, corresponding to the central visual field of the area

lateral

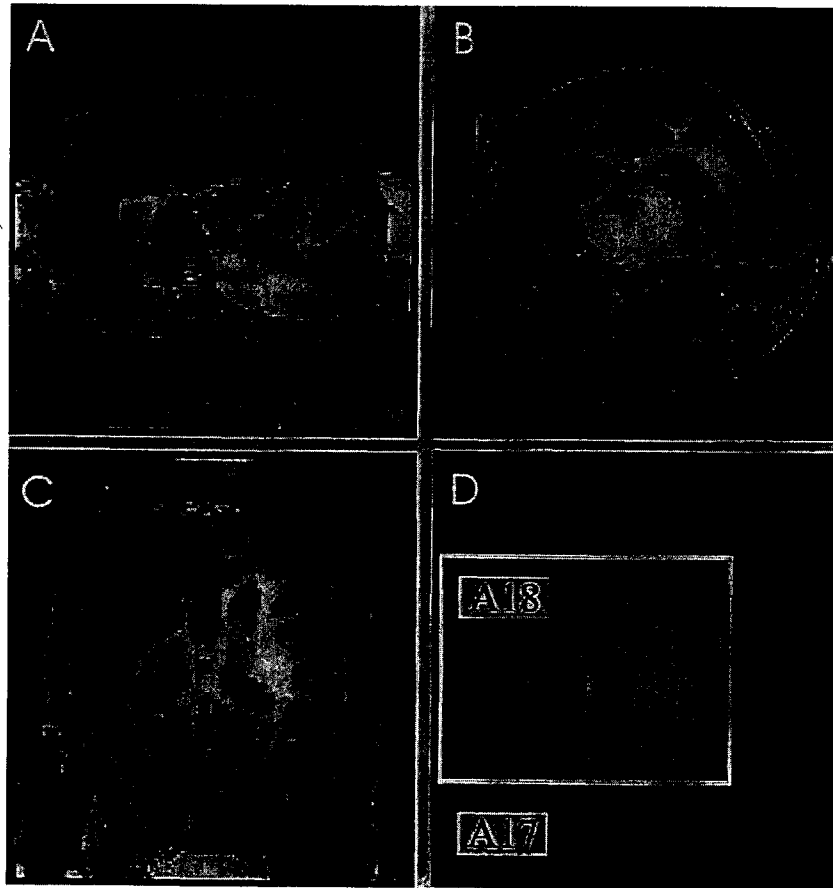
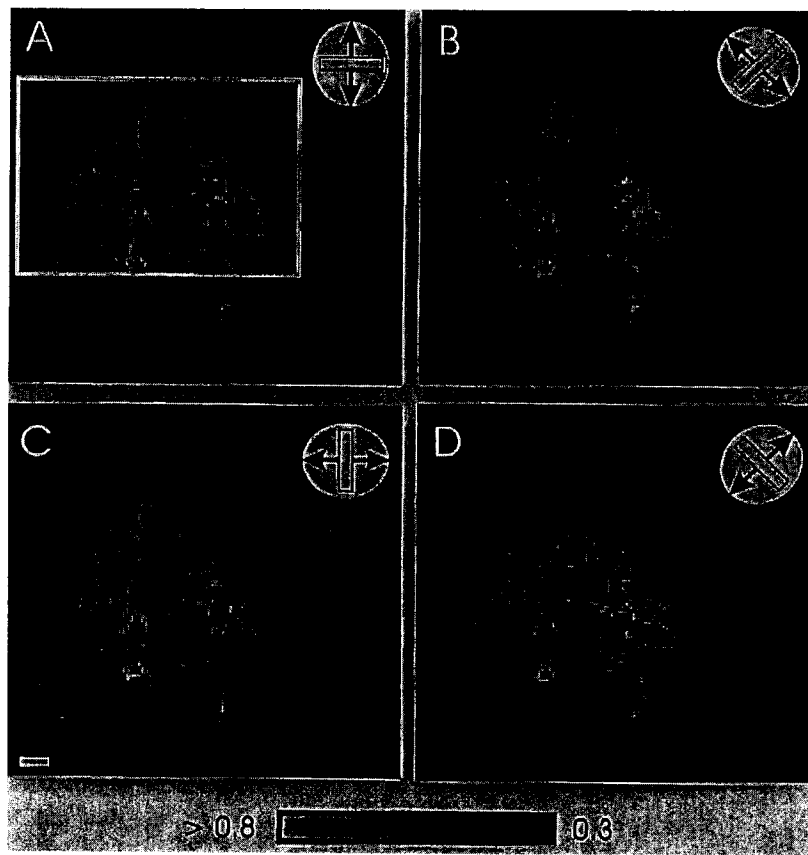


FIGURE 4-2. Mid-sagittal (A), coronal (B), and axial (C) anatomical images of the cat brain obtained with high-field magnet. The *sulcus cruciatus*, *sulcus splenialis*, and *sulcus suprasplenialis* are readily detectable on the mid-sagittal image. The white and gray matters in coronal and axial images are visible as bright and dark areas, respectively. Panel D displays the surface image of the left and right lateral gyri (left and right half of the image). The white box indicates the region of interest that has been used for the functional MR studies as described in this chapter. A17, area 17; A18, area 18.

18. The curved line at the right side of the panel is the lateral sulcus of the right hemisphere. Based on the pattern of sulci on the cortical surface, this particular cat was classified as to be a Otsuka-Hassler Type I cat (49).

All functional images described in this chapter were obtained from a region of interest (ROI) that corresponded to the white rectangle in Fig. 4-2D. BOLD measurements on a single image slice were made using gradient-echo, echo-planar imaging (EPI) technique (50,51). The imaging slice was positioned  $\sim 500 \mu\text{m}$  below pia to avoid superficial draining vessels. The MRI parameters were data



**FIGURE 4-3.** Functional MR images in cat primary visual cortex during stimulation of the animal with moving gratings of four different orientations. The regions of *increased* BOLD signal change are gray scale coded (bright = maximum BOLD signal). The numbers at the gray-scale key represent cross correlation coefficients. Robust and homogenous activities were observed in the lateral gyri of both hemispheres. The region of activity extended several millimeters in anteroposterior and medio-lateral directions. All four activation maps obtained in response to moving gratings of four different orientations ( $0^\circ$ ,  $45^\circ$ ,  $90^\circ$ ,  $135^\circ$ ) yielded homogeneous spatial distributions that were hardly distinguishable from each other. Scale bar: 1 mm.

#### Temporal Dynamics of BOLD

The most parsimonious explanation for these results can be found in the nature of the hemodynamic events during BOLD signal acquisition. Figure 4-4 summarizes, in a cartoon, the events following a hypothetical sensory stimulation.

Stimulation of the animal with moving gratings of a particular orientation, in this case  $90^\circ$ , will increase both the subthreshold and suprathreshold electrical activity among neurons located in the respective iso-orientation domains (see the left panel of Fig. 4-4). For the sake of simplicity, we assume the level of electrical activity in

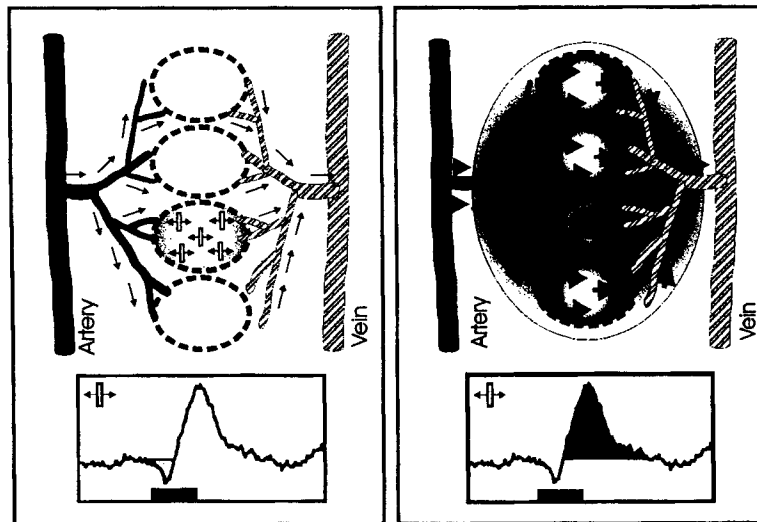


FIGURE 4-4. A "cartoon" summarizing the hemodynamic events following sensory stimulation. (Left panel) The hemodynamic events during the initial deoxygenation period. (Right panel) Hemodynamic events during the delayed oxygenation period. See text for details.

other columns—disregarding the lateral spread of activity through the plexus of horizontal connections—~~to~~ to remain more or less unchanged. The proposed hypothesis here is that the first event following increased neuronal activity will be a prolonged increase in oxygen consumption, caused by an elevation in oxidative metabolism of active neurons (58). Based on 2-DG data (26), we can assume the increase in oxidative metabolism in cat primary visual cortex to be colocalized with the site of electrical activity (see Chapter 3). The increase in oxidative metabolism will naturally elevate the local deoxyhemoglobin content in the parenchyma of active neurons, assuming there is no immediate commensurate change in cerebral blood flow (59). In  $T_2$  or  $T_2^*$ -weighted BOLD fMRI images, such increase in paramagnetic deoxyhemoglobin should be detectable as a transient *decrease* in observable MR signals (see the hypothetical time course in the left panel of Fig. 4-4).

Such an initial deoxygenation of the local cortical tissue (left panel) lasts only for a short time, as fresh blood (fresh oxyhemoglobin) rushes into capillaries in response to the increased metabolism (i.e., Roy and Sherrington's microcirculation response; see the right panel). Such increase in "fresh" oxyhemoglobin can be assumed to reverse the local ratio of hemoglobin in favor of oxyhemoglobin, thus resulting in an *increase* in observable MR signals. Obviously, this delayed oxygenation of the cortical tissue represents one of the bases for conventional BOLD signals (19).

Several lines of recent optical spectroscopy studies (41,42,60) suggest that, after sensory stimulation, such a "biphasic" response does indeed take place.

Their results indicate that the local deoxyhemoglobin concentration increases immediately after stimulation, yielding the maximum concentration about 2 to 3 seconds after stimulus onset. Oxygen consumption increase appears to be, at least in part, if not entirely, responsible for this early deoxyhemoglobin increase (61). The local deoxyhemoglobin concentration is subsequently reversed, ultimately resulting in a relatively large decrease in overall deoxyhemoglobin content.

The crucial question here is the “where” of the biphasic hemodynamic processes. To this end, it has been proposed that the two distinct hemodynamic events (initial deoxygenation followed by the delayed oxygenation) ought to result in fundamentally different functional specificity (41). It is assumed that the initial deoxygenation, as a consequence of an increase in oxidative metabolism, should be coregistered with the site of electrical activity up to the level of individual cortical columns. In fact, the well-established optical imaging of intrinsic signals (11,12), which has been cross-validated with single unit techniques (62–64), is similarly based on measuring the local transient increase of deoxyhemoglobin. The delayed oxygenation of the cortical tissue, on the other hand, is suggested to be far less specific. The assumption here is that the “fidelity” of the cortical vasculature is not sufficient to provide fresh oxyhemoglobin selectively to the active columns only. Instead, the entire local vicinity of the active column is flooded with fresh blood. Consequently, such delayed oxygenation signals, as detected with conventional BOLD technique, may surpass the spatial extent of the actual activated area by several millimeters (41,42).

Both the existence of “biphasic” BOLD response per se and the suggested differences in functional specificity continue to be debated. Although the initial deoxygenation signal in fMRI (termed *initial dip*) has been reported in humans (65–67) and monkeys (68), studies in rodents failed to detect any significant initial decrease in BOLD signal after sensory stimulation (69,70). Likewise, the spatial specificity of this dip remains unknown because most fMRI studies examining this phenomenon so far have been conducted in humans (65–67), thereby, by necessity using relatively coarse spatial resolution. In this context we need to address two crucial questions: (1) Are BOLD responses in cat primary visual cortex biphasic? (2) If so, does the initial deoxygenation signal label the layout of the cortical columns accurately, while the delayed oxygenation signals fail to discriminate individual cortical columns?

#### Cat Primary Visual Cortex—Biphasic responses?

Figure 4-5 demonstrates that, in cat primary visual cortex, the time evolution of MR signals is clearly biphasic. The temporal dynamics of the BOLD responses in cat primary visual cortex was in excellent agreement with optical spectroscopy data. After visual stimulation, the MR signal decreases, reaching a minimum of about  $-0.2$  to  $-0.4\%$  approximately 3 seconds after the stimulus onset. The signal then reverses, yielding a maximum positive signal change of 1.0 to 2.0% approximately 8 to 10 seconds after stimulus onset. Such biphasic BOLD responses after

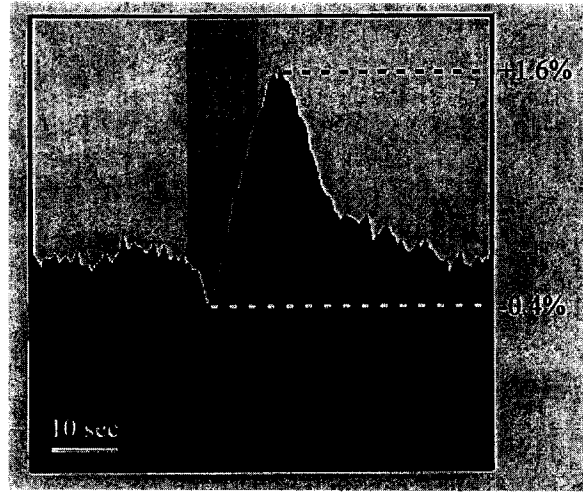


FIGURE 4-5. Biphasic time evolution of MR signals obtained in cat primary visual cortex. After visual stimulation, the MR signal decreases, reaching a minimum of about  $-0.2$ – $-0.4\%$  approximately 3 seconds after the stimulus onset. The signal then reverses, yielding a maximum positive signal change of  $1.0$ – $2.0\%$  approximately 8 to 10 seconds after stimulus onset. Scale bar: 10 seconds. (Adapted from Kim et al. [8].)

the visual stimulation were observed in all 10 experiments during the stimulation of the animal with moving gratings of different orientations (see Fig. 4-6). Furthermore, similar results were obtained at two different magnetic fields used for our studies (4.7 and 9.4T).

As the early negative signal changes are assumed to reflect the transient increase of local deoxyhemoglobin in parenchymal tissue, their use for functional map generation can be expected to greatly enhance the functional specificity of fMRI. To this end, to determine the time-dependent spatial layout of BOLD signals, the percent change maps within the negative and positive portions of BOLD time course were averaged into respective time-binned maps (positive and negative map, respectively). For the map of the negative response, individual pixels displaying negative percent change with at least 0.5 to 1.0 standard deviation away from the mean baseline percent change were taken to be statistically significant. For the positive response, the threshold was raised in proportion to contrast-to-noise ratio (CNR) of the maximum positive to the minimum negative BOLD response for each animal (i.e., about 5 times).

Figure 4-7 shows that the initial deoxygenation and the delayed oxygenation signals yield a fundamentally different pattern of activity in response to identical visual stimulus. Panel A depicts the spatial pattern of increased BOLD activity in response to moving gratings of  $45^\circ$  orientation. The positive BOLD percent changes are coded with gray scales as indicated by the respective key below. Similar to activation maps

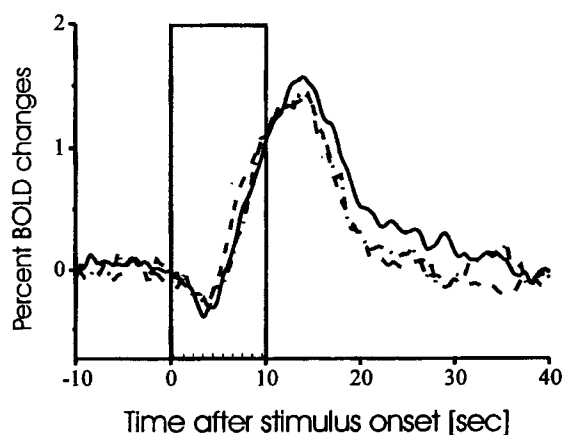


FIGURE 4-6. Biphasic BOLD responses following the visual stimulation were observed in all 10 experiments at two different magnetic fields. The depicted MR time courses represent the biphasic responses obtained during the stimulation of the animal with moving gratings of different orientations. The stimulus duration is marked by the inset rectangle. (Adapted from Duong et al. [73].)

based on conventional cross-correlation analysis (Fig. 4-3), robust and homogenous activities were observed from the entire ~~marginal~~ <sup>lateral</sup> gyrus of both hemispheres. The region of activity extended several millimeters in anteriorposterior and mediolateral directions. The pattern of activity based negative BOLD percent changes (Fig. 4-7B), on the other hand, yielded strikingly different spatial layout. Here, the gray-scale coded pixels represent regions of significant decrease in MR signals after visual stimulation. In sharp contrast to the conventional fMRI maps based on positive BOLD signal changes, the foci of the negative signal changes are confined to patchy clusters. In line with the iso-orientation columns in cat primary visual cortex observed using 2-DG (26) and optical imaging (5,5) techniques, such semiellipsoidal and irregularly shaped clusters are distributed all over the approximated area 18, with an average periodicity of about  $1.34 \pm 0.23$  mm. Note also how the areas defined by negative signal changes are located largely in tissue areas only, avoiding regions of large blood vessels including the region around the sagittal sinus.

Although the data in Fig. 4-7 indicate that the initial deoxygenation signals yield a far more column-like pattern of activity compared with those based on conventional positive BOLD signals, important questions remain to be addressed. For example, given the large difference in absolute amplitude between the negative and positive signals (Fig. 4-5), it is conceivable that the differences in spatial pattern between the positive (Fig. 4-7A) and negative (Fig. 4-7B) maps could be due simply to the difficulty in equating the signal threshold levels. We have addressed this possibility by raising the threshold for the positive response to match the number of "activated" pixels in both maps. The resulting positive map (Fig. 4-8B) largely reflects the surface vasculature pattern of the visual cortex, with the strongest signals originating from the sagittal sinus.



**FIGURE 4-7.** Improvement of spatial specificity of BOLD using the initial negative signal changes. (A) The pattern of increased BOLD activity in response to moving gratings of  $45^\circ$  orientation. The positive BOLD percent changes are marked with gray scales as indicated by the gray scale key below. For the functional map displayed in panel (B), only negative BOLD percent changes occurring within the first 2 seconds after stimulus onset were utilized. The gray-scale key below indicates the negative percent changes. See text for details. Scale bar for panels: 1 mm. (Adapted from Kim et al. [8].)

These results clearly demonstrate that the differences in spatial pattern between the map of negative and positive responses are genuine. Furthermore, results in Figs. 4-7 and 4-8 show that there is no method of linear thresholding that will yield columnar pattern of activity based on positive BOLD responses. If a low threshold is used, the resulting map will be homogenous, with no differences between functional maps obtained for different receptive field properties (Fig. 4-3). Choosing a

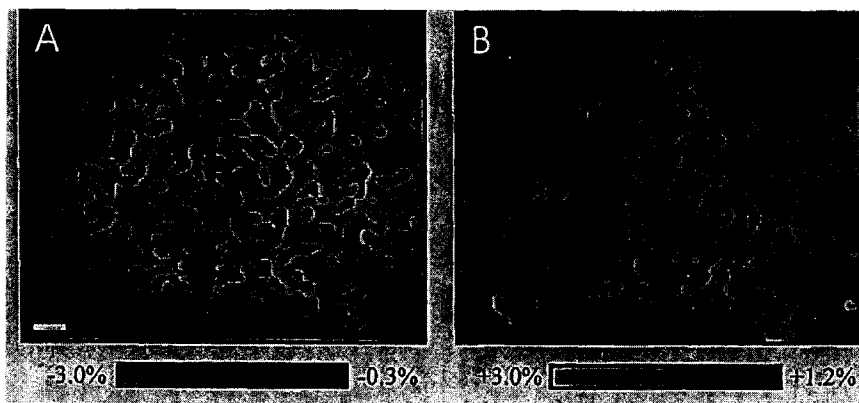


**FIGURE 4-8.** Differences in spatial layout of activity based on negative (A) and positive (B) BOLD responses. For this comparison, the threshold for the positive response was raised to match the number of activated pixels in the negative map (A). The resulting positive map (B) reflects largely the surface vasculature pattern of the visual cortex. Scale bar: 1 mm. (Adapted from Kim et al. [8].)

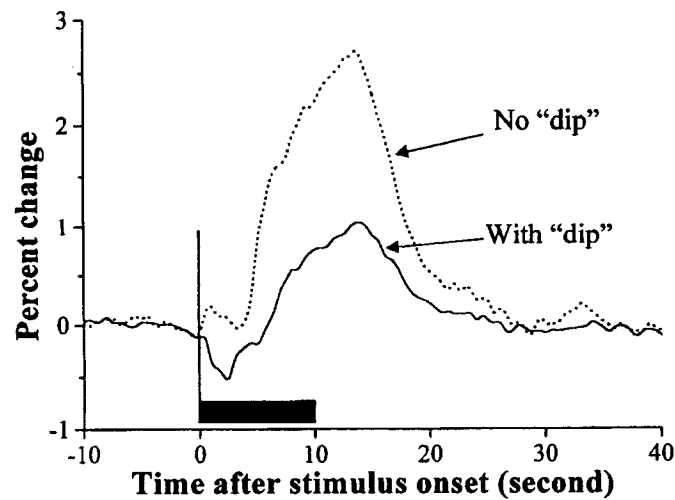


FIGURE 4-9. Expanded time courses for the pixels that exhibit early negative (solid line) and no early negative (dash line) responses, respectively. Stimulus duration is marked with the black box. Note that the pixels, which did not exhibit an early negative response, produced a much larger delayed positive response than those with an early negative response. See text for more details. (Adapted from Duong et al. [73].)

high threshold on the other hand results in activated pixels that represent predominantly nonfunctional draining vessels (Fig. 8B). This notion is further corroborated in Fig. 4-9. Here, the image pixels were classified into two disjoint sets: pixels exhibiting an initial dip response (dip-pixels) and those with no such responses (nodip-pixels). If we plot the entire signal time courses for these two groups of pixels (Fig. 4-9), it is clear that the nodip-pixels exhibit a much larger positive BOLD response than those from dip-pixels. If we assume the nodip-pixels to largely represent draining vessel signals, then choosing a high threshold in conventional BOLD fMRI, for the sake of improved statistics, may do just the opposite of what was intended, namely, selecting non-functional signals only.

#### Functional Properties of "Negative BOLD" Signals in Cat Primary Visual Cortex

We have found that the initial negative BOLD signals yield, in sharp contrast to positive signals, a column-like pattern of activity in which activated pixels are clustered into isofunctional domains with a periodicity of about 1 mm (Fig. 4-7). The crucial question is whether those column-like domains represent genuine iso-orientation domains. To this end, the ultimate validation of the veracity of the fMRI-based iso-orientation columns requires simultaneous recording of single ~~units~~ *unit activity*. Such simultaneous recording requires the recording setup to be placed around the isocenter of the magnetic bore, resulting in devastating magnetic field

interferences. Furthermore, in such a design, it is almost impossible to change the electrode track or introduce new electrodes without repositioning the animal. ~~Therefore, it seems unlikely that a direct electrophysiological validation of our fMRI columns could be carried out at this point.~~

Although many groups (including our own group) are vigorously trying to overcome the technical difficulties to ensure a direct electrophysiological validation of the functional MR data, we reasoned it worthwhile to attempt a more "indirect" validation of our MR-derived columns. We took advantage of the fact that the spatial layout of the orientation columns in cat primary visual cortex displays a set of characteristic features that is well established (13,14). For example, it is well known that the orientation domains for orthogonal orientations are complementary. In fact we have used this complementary criteria in our assessment of the positive BOLD maps (Fig. 4-3).

Figure 4-10 depicts the results of such a complementarity test for negative BOLD data. Panels A through D display patterns of negative activity obtained from the same patch of cortex during the stimulation of the animal with the four different orientation stimuli. Analogous to 2-DG (26) and optical imaging (16),

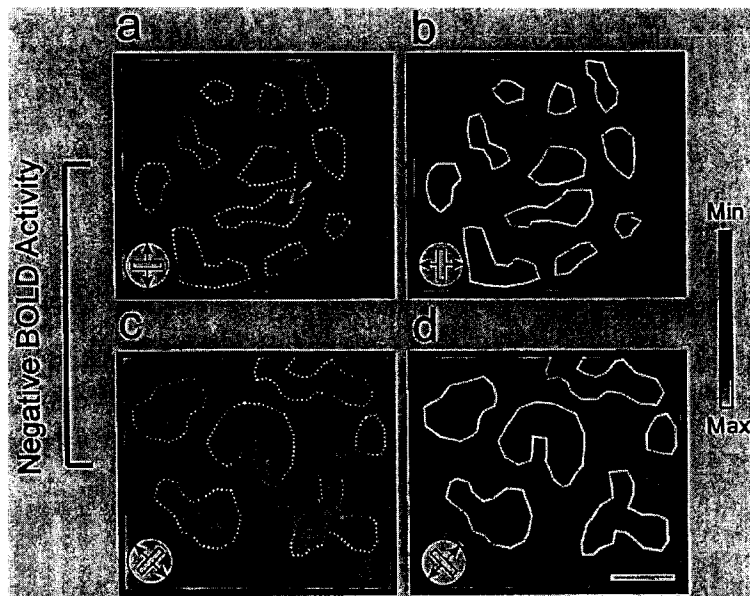


**FIGURE 4-10.** Representation of orthogonal orientations in complementary cortical domains. (A-D) Patterns of "negative" activity in response to four orientations ( $0^\circ$ ,  $45^\circ$ ,  $90^\circ$ ,  $135^\circ$ ). Regions of negative signal changes during the first 2 seconds after visual stimulation are displayed as dark pixels. For visual inspection of the complementarity between the orthogonal orientation maps, the patches in panels (B) and (D) are outlined and overlaid on the maps in panels (A) and (C), respectively. Other than a few exceptions (marked with an arrowhead), the maps for orthogonal orientations are complementary to each other. Scale bar: 1 mm. (Adapted from Kim et al. [8].)

Figure 4-10

regions of high activity (i.e., large negative signals) are displayed as dark pixels. For removing the effects of uneven MR signals across the cortical surface, the conventional "cocktail blank" method was used (16). It is evident that each pattern of negative activity is highly specific to the respective stimulus orientation. To corroborate this notion, the outlines of the orientation patches for  $90^\circ$  and  $135^\circ$  maps are overlaid on the maps obtained for the respective "orthogonal" orientations (Fig. 10). It is clear from these panels that the patches for orthogonal orientations occupy cortical territories that are mostly complementary.

The ability of the negative BOLD signals to reflect the stimulus selective responses at columnar scale is further elucidated in Fig. 4-11. Here, the left and right panels represent the signal time courses obtained from  $45^\circ$  (solid time courses) and  $135^\circ$  (dashed time courses) orientation columns, respectively. It is clear that MR signals in pixels representing  $45^\circ$  columns decreased transiently during the  $45^\circ$  stimulation (left panel), while little or no such decrease was observed during the  $135^\circ$  stimulation (right panel). Likewise, MR signals from  $135^\circ$  columns decreased transiently during the  $135^\circ$  stimulation, but not during the complementary  $45^\circ$  stimulation.

The positive BOLD signals, on the other hand, were much less suited to discriminate between  $45^\circ$  and  $135^\circ$  columns, as they yielded largely overlapping times courses for both stimulus conditions (see the overlapping signals in either panels during the positive periods).

Finally, to permit a more direct comparison of the map quality, we have also calculated the  $45^\circ$  and  $135^\circ$  maps obtained during the positive BOLD period (Fig. 4-

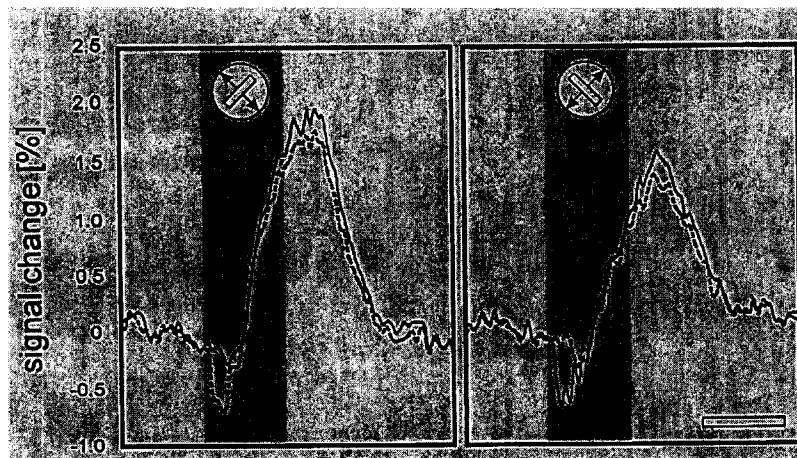


FIGURE 4-11. The signal time courses for  $45^\circ$  (dashed time course) and  $135^\circ$  (solid time course) columns during the stimulation with  $45^\circ$  (left panel) and  $135^\circ$  (right panel) orientation stimuli. The stimulation duration of 10 seconds is marked in both panels by the gray boxes behind the time courses. See text for more details. Scale bar: 10 seconds. (Adapted from Kim et al. [8].)

12). All functional maps depicted in Figs. 4-10 and 4-12 were acquired in the same fMRI studies, and analogous methods of image processing have been applied. In contrast to the patchy and interdigitized columns in negative maps, the domains of the positive BOLD responses are larger with no apparent periodicity. The outlines of the 135° map from Fig. 4-3B were then overlaid on the 45° map (Fig. 4-12A). The regions of positive activity for the orthogonal orientations were mostly overlapping.

The results shown in Figs. 4-10 through 4-12 are interesting for two reasons. First, the complementarity of the negative BOLD maps obtained during the stimulation with orthogonal orientation further corroborates the notion that the MR-based “columns” may indeed represent genuine iso-orientation columns. Furthermore, the results in Figs. 4-10 through 4-12 suggest that, although the nominal amplitude of the negative signals is far smaller than that of the positive signals (Fig. 4-5-6), the *stimulus specific contrast* of the negative signals was found to be far superior to that of the positive signals. Based on Figs. 4-10 through 4-12, we estimate the stimulus-specific contrast of the negative signals to be about 6.5 times larger compared with that of the positive signals.

#### fMRI-Based Pinwheels

Finally, as a further way of indirect validation, we attempted to derive the distinct topology of the composite orientation map in cat primary visual cortex using

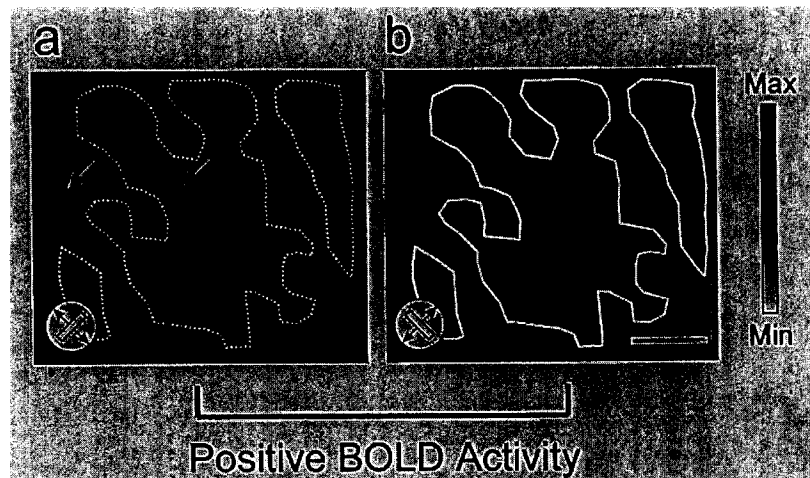


**FIGURE 4-12.** Representation of orthogonal orientations in positive BOLD maps. (A,B) Functional maps based on positive signal changes obtained during the stimulation of the animal with 45° and 135°, respectively. High positive signals are represented by dark pixels. The domains of high activity in 135° map (B) are outlined and overlaid on the 45° map (A). Most of the active domains in both maps are overlapping extensively. However, a few prominent exceptions exist (marked with arrowheads). Scale bar: 1 mm. (Adapted from Kim et al. [8].)

our negative BOLD maps. A characteristic and invariant feature of the mammalian orientation system is the existence of topological singularities (16) that were observed across many mammalian species using both multielectrode (7,71) and optical imaging (16) techniques.

With the use of our negative BOLD fMRI data, we obtained composite angle maps for the negative BOLD changes through a pixel-by-pixel vector addition of the four iso-orientation maps with the negative percent changes as vector amplitudes and the respective stimulus orientations as vector angles. The resulting angle at each pixel was then coded using a gray-scale code (Fig. 4-13).

In the composite map based on the early negative BOLD signals only (Fig. 4-13A), the preferred orientations change smoothly, forming a map of orientation

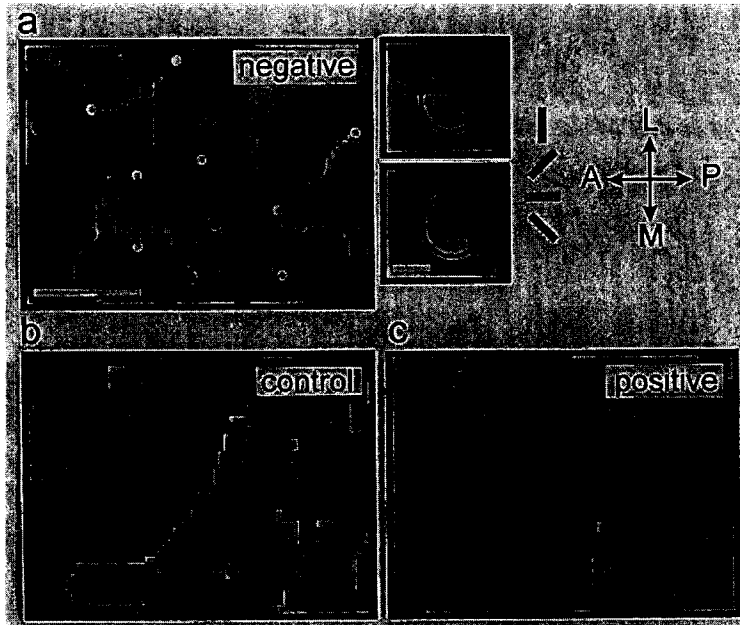


**FIGURE 4-13.** fMRI-based composite-angle maps. (A) The composite-angle map obtained through pixel-by-pixel vector addition of the four single iso-orientation maps based on negative signal changes. The gray scale key next to (A) was used for gray-scale coding the resulting orientation preferences. The overall continuity of the orientation preferences is interrupted at the orientation pinwheels where the cortical columns for different orientations are arranged in a circular manner. The white and black circles in panel (A) depict such clockwise and counterclockwise pinwheels, respectively. Two of such pinwheels are displayed, enlarged right to panel (A). Scale bar for the enlarged pinwheels: 200  $\mu$ m. As a control, the composite maps based on MR signals obtained before stimulus onset (B) and during positive BOLD signals (C) are also displayed. The maps in (B) and (C) were obtained from the identical cortical region as displayed in panel (A). The control maps are devoid of topological structures that are characteristic for genuine composite angle maps. Scale bar for (A-C): 1 mm. A, anterior; P, posterior; M, medial; L, lateral. (Adapted from Kim et al. [8].)

selectivity. The continuity of orientation preferences is interrupted only at the singular points (termed orientation pinwheels) where the domains for all orientations converge, in a way analogous to that obtained using multielectrode and optical imaging techniques. Each orientation is represented only once around such a pinwheel, thereby forming two types of topological singularities according to their rotational chiralities. Two of such pinwheels are depicted enlarged to the right of Fig. 4-13A. The pinwheel density and the ratio between clockwise and counterclockwise singularities found in negative BOLD composite maps were in excellent agreement with those obtained with optical imaging techniques. In our study, a pinwheel density of  $1.46 \pm 0.17$  pinwheels/mm<sup>2</sup> was found, and optical imaging studies (5,62) yielded average pinwheel densities between 1.2 and 1.95 pinwheels/mm<sup>2</sup>. Likewise, the ratio between clockwise and counterclockwise pinwheels was found to be roughly 1:1 in both negative-BOLD and optical imaging data (see Chapter 2).

Although the preceding data agree with data from multielectrode and optical imaging studies, it is theoretically possible, that topological singularities could arise from a randomly distributed pattern of activity (72). Therefore, as a control, composite maps based on signals obtained before stimulus onset (Fig. 4-13B), and those during the delayed positive BOLD changes (Fig. 4-13C) were also calculated. All steps for composite map construction were performed identical to that for Fig. 4-13A. Unlike the composite map based on negative BOLD signals (Fig. 4-13A), the maps based on control (Fig. 4-13B) or delayed positive BOLD signals (Fig. 4-13C) displayed none of the characteristic features of the mammalian angle maps.

## CONCLUSIONS

Our results from cat primary visual cortex clearly indicate that the functional specificity of BOLD at columnar scale depends highly on the temporal dynamics of the underlying signals (73). If the early negative signals are used, functional maps at columnar resolution can be obtained without the need of differential imaging (see later). The delayed positive BOLD changes, on the other hand, were clearly indicative for the pattern of the overall activation per se in the visual cortex, but were less suited to discriminate between the active and inactive columns, as they were more diffused and were less specific for the individual stimulus properties.

It is conceivable that, in principle, even such diffused positive BOLD signals could yield columnar pattern of activity, if maps of orthogonal conditions are subtracted from each other. Such differential imaging had been suggested for analyzing optical imaging (74), and conventional (i.e., positive) BOLD data (75). Although the use of differential method for optical imaging data might be defensible given the well-established verification of intrinsic signals with extensive single unit studies (62,64), the use of differential method for BOLD fMRI data, however, poses severe difficulties. In differential imaging, one activation map (e.g., to

the left eye) is subtracted by the activity map that is assumed to give the complementary activation pattern (e.g., to the right eye). If this assumption is true—such as between left- and right-eye domains—then the result of the subtraction is tautological, as it was known in advance. If the assumption is not true, however, or simply not known, as for most receptive field properties, then the subtraction method may give the wrong answer. Lacking the direct validation of BOLD using simultaneous single unit recordings to date, the applicability of the differential method for BOLD data must remain questionable.

$T_2^*$  As the  $T_2$  and  $T_2^*$  weighted BOLD contrast predominantly originates from the regional changes in paramagnetic deoxyhemoglobin concentration (18,27), the early decrease of BOLD signals can most likely be attributed to the regional increase of deoxyhemoglobin after neuronal stimulation. Although alternative explanations exist (76), the most parsimonious explanation for such a transient deoxygenation is a transient increase in oxygen gradients from the capillaries to the tissues caused by an increase in oxygen consumption within the active orientation column without a commensurate increase in blood flow (41,42,61).

Early, transient decrease in BOLD signals has also been observed in the cortices of awake human (65–67,77) and anesthetized nonhuman primates (68) during perceptual tasks, indicating that, in principle, the capability of BOLD-fMRI to label functional columns in vivo should be applicable also in humans and monkeys. The upcoming challenge in human studies will be to attain stable and sufficient signal-to-noise-ratio from subcolumnar sized voxels, which is more difficult to achieve in awake humans than from anesthetized small animals.

Future studies in cat visual cortex will take full advantage of this novel MRI method (e.g., noninvasivity and depth resolution) to elucidate the layer-specific development and plasticity of the functional organization in multiple visual areas within the same animal. Furthermore, recent advances in diffusion tensor MRI (78) promises that high-resolution mapping of the axonal connectivity in cat visual cortex can be achieved in a completely noninvasive manner (79). Combined with columnar-resolution fMRI (8,73), this would pose a powerful new paradigm that would make it possible for the pattern of functional activity to be directly correlated with that of the underlying neuronal circuitry in a *living* animal.

As with any new technique, this novel method for noninvasive visualization of cortical columns by fMRI will naturally need further improvements and cross-validations (see Kim et al. [80] for initial attempts). We can conclude from our study, however, that noninvasive fMRI of brain functions can now be performed at columnar levels, thus bridging the gap between neurophysiology and cognitive sciences.

#### ACKNOWLEDGEMENTS

$\checkmark$   $\text{ing}$   
We thank Dr. H. Merkle and J. Strupp provided supports in hard- and software. We would also like thank Drs. R. Galuske, R. Goebel, and I. Ronen helpful discussions. This work was supported by the NIH (NS38295, MH57180, NS10930, RR08079), the Minnesota Medical Foundation, and the Keck Foundation.

QUERY  
SEE MS PAGE

65. Menon, R. S., Ogawa, S., Hu, X., Strupp, J. P., Anderson, P., and Ugurbil, K. (1995). BOLD based functional MRI at 4 Tesla *includes* a capillary bed contribution: Echo Planar Imaging correlates with previous optical imaging using intrinsic signals. *Magn. Reson. Med.* **33**, 453-459.
66. Hu, X., Le, T. H., and Ugurbil, K. (1997). Evaluation of the early response in fMRI in individual subjects using short stimulus duration. *Magn. Reson. Med.* **37**, 877-884.
67. Yacoub, E., and Hu, X. (1999). Detection of the early negative response in fMRI at 1.5 Tesla. *Magn. Reson. Med.* **41**, 1088-1092.
68. Logothetis, N. K., Guggenberger, H., Peled, S., and Pauls, J. (1999). Functional imaging of the monkey brain. *Nat. Neurosci.* **2**, 555-562.
69. Marota, J. J. A., Ayata, C., Moskowitz, M. A., Weisskopf, R. M., Rosen, B. R., and Mandeville, J. B. (1999). Investigation of the early response to rat forepaw stimulation. *Magn. Res. Med.* **41**, 247-252.
70. Silva, A. C., Lee, S.-P., Iadecola, C., and Kim, S.-G. (2000). Early characteristics of CBF and deoxyhemoglobin changes during somatosensory stimulation. *J. Cereb. Blood Flow Metab.* **20**, 201-205.
71. Diao, Y. C., Jia, W. G., Swindale, N. V., and Cynader, M. S. (1990). Functional organization of the cortical 17/18 border region in the cat. *Exp. Brain Res.* **79**, 271-282.
72. Rojer, A. S., and Schwartz, E. L. (1990). Cat and monkey cortical columnar patterns modeled by bandpass-filtered 2D white noise. *Biol. Cybern.* **62**, 381-391.
73. Duong, T. Q., Kim, D.-S., Ugurbil, K., and Kim, S.-G. (2000). Spatio-temporal dynamics of BOLD fMRI signals: towards mapping submillimeter cortical columns using the early negative response. *Magn. Reson. Med.* **44**, 231-242.
74. Blasdel, G. G. (1992). Differential imaging of ocular dominance and orientation selectivity in monkey striate cortex. *J. Neurosci.* **12**, 3115-3138.
75. Menon, R. S., Ogawa, S., Strupp, J. P., and Ugurbil, K. (1997). Ocular dominance in human V1 demonstrated by functional magnetic resonance imaging. *J. Neurophysiol.* **77**, 2780-2787.
76. Buxton, R. B., and Frank, L. R. (1997). A model for the coupling between cerebral blood flow and oxygen metabolism during neural stimulation. *J. Cereb. Blood Flow Metab.* **17**, 64-72.
77. Ernst, T., and Henning, J. (1994). Observation of a fast response in functional MR. *Magn. Reson. Med.* **32**, 146-149.
78. Xue, R., van Zijl, P. C. M., Crain, B. J., Solaiyappan, M., and Mori, S. (1999). In vivo three-dimensional reconstruction of rat brain axonal projections by diffusion tensor-imaging. *Magn. Reson. Med.* **42**, 1123-1127.
79. Mori, S., Ugurbil, K., van Zijl P. C. M., and Kim D.-S. (2000). In vivo mapping of the axonal connectivity in cat visual cortex using diffusion tensor MRI. *Soc. Neurosci. Abstr.* **550.1**
80. Kim, D.-S., Duong, T. Q., Ronen, I., Ugurbil, K., and Kim, S.-G. (2000). Neural correlate of blood oxygenation level dependent functional MRI. *Soc. Neurosci. Abstr.* **309.6**

## REFERENCES

1. Brodmann, K. (1909). *Vergleichende Lokalisationslehre der Grosshirnrinde*. Leipzig, Verlag von Johann Ambrosius Barth.
2. Hubel, D. H., and Wiesel, T. N. (1962). Receptive field, binocular interactions and functional architecture in the cat's visual cortex. *J. Physiol. (Lond)* **160**, 106–154.
3. LeVay, S., Stryker, M. P., and Shatz, C. J. (1978). Ocular dominance columns and their development in layer IV of cat's visual cortex. *J. Comp. Neurol.* **179**, 223–244.
4. Hubel, D. H., Wiesel, T. N., and Stryker, M. P. (1978). Anatomical demonstration of orientation columns in macaque monkey. *J. Comp. Neurol.* **177**, 361–380.
5. Bonhoeffer, T., and Grinvald, A. (1991). Iso-orientation domains in cat visual cortex are arranged in pinwheel-like pattern. *Nature* **353**, 429–432.
6. Payne, B. R., Berman, N. E. J., and Murphy, E. H. (1981). Organization of direction preference in cat visual cortex. *Brain Res.* **211**, 445–450.
7. Swindale, N. W., Matsubara, J. A., and Cynader, M. S. (1987). Surface organization of orientation and direction selectivity in cat area 18. *J. Neurosci.* **7**, 1414–1427.
8. Kim, D.-S., Duong, T. Q., and Kim, S.-G. (2000). Mapping iso-functional columns using magnetic resonance imaging. *Nat. Neurosci.* **3**, 164–169.
9. LeVay, S., and Nelson, S. B. (1991). Columnar organization of the visual cortex. In: *The neurological basis of visual function and visual dysfunction* (J. Cronly-Dillon, and A. G. Leventhal, Eds.), pp. 266–315, Boca Raton, CRC Press.
10. Sokoloff, L., Reivich, M., Kennedy, C., DesRosiers, M. H., Patlak, C. S., Pettigrew, K. D., Sakurada, O., and Shinohara, M. (1977). The 14C-deoxyglucose method for the measurement of local cerebral glucose utilization: theory, procedure, and normal values in the conscious and anesthetized albino rat. *J. Neurochem.* **28**, 897–916.
11. Grinvald, A., Lieke, E., Frostig, R. D., Gilbert, C. D., and Wiesel, T. N. (1986). Functional architecture of cortex revealed by optical imaging of intrinsic signals. *Nature* **324**, 361–364.
12. Frostig, R. D., Lieke, E. E., Ts'o, D. Y., and Grinvald, A. (1990). Cortical functional architecture and local coupling between neuronal activity and the microcirculation revealed by in vivo high-resolution optical imaging of intrinsic signals. *Proc. Natl. Acad. Sci. U.S.A.* **87**, 6082–6086.
13. Huebener, M., Shoham, D., Grinvald, A., and Bonhoeffer, T. (1997). Spatial relationships among three columnar systems in cat area 17. *J. Neurosci.* **17**, 9270–9284.
14. Kim, D.-S., Matsuda, Y., Ohki, K., Ajima, A., and Tanaka, S. (1999). Geometrical and topological relationships between multiple functional maps in cat primary visual cortex. *Neuroreport* **10**, 2515–2522.
15. Yae H., Elias, S. A., and Ebner, T. J. (1992). Deblurring of 3-dimensional patterns of evoked rat cerebellar cortical activity: a study using voltage-sensitive dyes and optical sectioning. *J. Neurosci. Methods* **42**, 195–209.
16. Bonhoeffer, T., and Grinvald, A. (1993). The layout of iso-orientation domains in area 18 of cat visual cortex: optical imaging reveals a pinwheel-like organization. *J. Neurosci.* **13**, 4157–4180.
17. Stetter, M., and Obermayer K. (1999). Simulation of scanning laser technique for optical imaging of blood-related intrinsic signals. *J. Opt. Soc. Am. A. Opt. Image. Sci. Vis.* **16**, 58–70.
18. Ogawa, S., Lee, T. M., Nayak, A. S., and Glynn, P. (1990). Oxygenation-sensitive contrast in magnetic resonance image of rodent brain at high magnetic fields. *Magn. Reson. Med.* **14**, 68–78.
19. Ogawa, S., Tank, D., Menon, R., Ellermann, J. M., Kim, S.-G., Merkle, K., and Ugurbil, K. (1992). Intrinsic signal changes accompanying sensory stimulation: functional brain mapping using MRI. *Proc. Natl. Acad. Sci. U.S.A.* **89**, 5951–5955.
20. Wagner, A. D., Schacter, D. L., Rotte, M., Koutstaal, W., Maril, A., Dale, A. M., Rosen, B. R., and Buckner, R. L. (1998). Building memories: remembering and forgetting of verbal experiences as predicted by brain activity. *Science* **281**, 1188–1191.
21. Kim, S.-G., Ashe, J., Hendrich, K., Ellermann, J. M., Merkle, H., Ugurbil, K., and Georgopoulos, P. (1993). Functional magnetic resonance imaging of motor cortex: hemispheric asymmetry and handedness. *Science* **262**, 615–617.

magnetic

- human |
22. DeYoe, E. A., Carman, G. J., Bandettini, P., Glickman, S., Wieser, J., Coy, R., Miller, D., and Neitz, J. (1996). Mapping striate and extrastriate visual areas in human cerebral cortex. *Proc. Natl. Acad. Sci. U.S.A.* **93**, 2382–2386.
  23. Engel, A. S., Glover, G. H., and Wandell, B. A. (1997). Retinotopic organization in human visual cortex and the spatial precision of functional MRI. *Cereb. Cortex* **7**, 181–192.
  24. Tootell, R. B., Mendola, J. D., Hadjikhani, N. K., Ledden, P. J., Liu, A. K., Reppas, J. B., Sereno, M. I., and Dale, A. M. (1997). Functional analysis of V3A and related areas in monkey visual cortex. *J. Neurosci.* **17**, 7070–7078.
  25. Wandell, B. (1999). Computational neuroimaging of human visual cortex. *Annu. Rev. Neurosci.* **22**, 145–173.
  26. Loewel, S., Freeman, B., and Singer, W. (1987). Topographic organization of the orientation column system in large, flat-mounts of the cat visual cortex: a 2-deoxyglucose study. *J. Comp. Neurol.* **255**, 401–415.
  27. Ogawa, S., Menon, R. S., Kim, S.-G., and Ugurbil, K. (1998). On the characteristics of functional magnetic resonance imaging of the brain. *Annu. Rev. Biophys. Biomol. Struct.* **27**, 447–474.
  28. Rabi, I. I., Zacharias, J. R., Millman, S., and Kusch, P. (1938). A new method of measuring nuclear magnetic moment. *Phys. Rev.* **53**, 318.
  29. Bloch, F., Hansen, W. W., and Packard, M. (1946). The nuclear induction experiment. *Phys. Rev.* **70**, 474–485.
  30. Lauterbur, P. C. (1973). Image formation by induced local interaction: examples employing nuclear magnetic resonance imaging. *Nature* **241**, 190–191.
  31. Belliveau, J. W., Kennedy, D. N., McKinstry, R. C., Buchbinder, B. R., Weisskoff, R. M., Cohen, M. S., Vevea, J. M., Brady, T. J., and Rosen, B. R. (1991). Functional mapping of the human visual cortex by magnetic resonance imaging. *Science* **254**, 716–719.
  32. Rosen, B. R., Belliveau, J. W., Aron, H. J., Kennedy, D., Buchbinder, B. R., Fischman, A., Gruber, M., Glas, J., Weisskoff, R. M., Cohen, M. S., Hochberg, F. H., and Brady, T. J. (1991). Susceptibility contrast imaging of cerebral blood volume: human experience. *Magn. Reson. Med.* **22**, 293–299.
  33. Bandettini, P. A., Wong, E. C., Hinks, R. S., Tikofsky, R. S., and Hyde, J. S. (1992). Time course EPI of human brain function during task activation. *Magn. Reson. Med.* **25**, 390–398.
  34. Kwong, K. K., Belliveau, J. W., Chesler, D. A., Goldberg, I. E., Weisskoff, R. M., Poncelet, B. P., Kennedy, D. N., Hoppel, B. E., Cohen, M. S., Turner, R., Cheng, H. M., Brady, T. J., and Rosen, B. R. (1992). Dynamic magnetic resonance imaging of human brain activity during primary sensory stimulation. *Proc. Natl. Acad. Sci. U.S.A.* **89**, 5675–5679.
  35. Pauling, L., and Coryell, C. D. (1936). The magnetic properties and structure of hemoglobin, oxy-hemoglobin, and carbonmonoxyhemoglobin. *Proc. Natl. Acad. Sci. U.S.A.* **22**, 210–216.
  36. Thulborn, K. R., Waterton, J. C., Matthews, P. M., and Radda, G. K. (1982). Dependence of the transverse relaxation time of water protons in whole blood at high field. *Biochem. Biophys. Acta* **714**, 265–272.
  37. Roy, C. S., and Sherrington, C. S. (1890). On the regulation of blood supply of the brain. *J. Physiol.* **11**, 85–108.
  38. Pawlik, G. Rackle, A., and Bing, R. J. (1981). Quantitative capillary topography and blood flow in the cerebral cortex of cat: an in vivo microscopic study. *Brain Res.* **208**, 35–58.
  39. Lai, S., Hopkins, A. L., Haacke, E. M., Li, D., Wasserman, B. A., Buckley, P., Friedman, L., Meltzer, H., Hedera, P., and Friedland, R. (1993). Identification of vascular structures as a major source of signal contrast in high resolution 2D and 3D functional activation imaging of the motor cortex at 1.5T: preliminary results. *Magn. Reson. Med.* **30**, 387–392.
  40. Menon, R. S., Hu, X., Adriany, G., Petersen, P., Ogawa, S., and Ugurbil, K. (1994). Comparison of spin-echo EPI, asymmetric spin-echo EPI and conventional EPI applied to functional neuroimaging: the effect of flow crushing gradients on the BOLD signal. *Proc. 2nd Soc. Magn. Reson.*, 622.
  41. Malonek, D., and Grinvald, A. (1996). Interactions between electrical activity and cortical microcirculation revealed by imaging spectroscopy: Implication for functional brain mapping. *Science* **272**, 551–554.

activity

42. Malonek, D., Dirnagl, U., Lindauer, U., Yamada, K., Kanno, I., and Grinvald, A. (1997). Vascular imprints of neuronal activity: relationships between the dynamics of cortical blood flow, oxygenation, and volume changes following sensory stimulation. *Proc. Natl. Acad. Sci. U.S.A.* **94**, 14826–14831.
43. Shmuel, A., Hu, X., Ugurbil, K., and Grinvald, A. (2000). Spread of hemo-dynamic signals in draining veins beyond the regions of electrical activation. *Proc. 8th Soc. Magn. Reson.*, 979.
44. Weisskoff, R. M., Zuo, C. S., Boxerman, J. L., and Rosen, B. R. (1994). Microscopic susceptibility variation and transverse relaxation: theory and experiment. *Magn. Reson. Med.* **31**, 601–610.
45. Song, A. W., Wong, E. C., Tan, S. G., and Hyde, J. S. (1996). Diffusion weighted fMRI at 1.5 T. *Magn. Reson. Med.* **35**, 155–158.
46. Ugurbil, K., Hu, X., Wei, C., Zhu, X.-H., Kim, S.-G., and Georgopoulos, A. (1999). Functional mapping in the human brain using high magnetic fields. *Philos. Trans. R. Soc. Lond. Biol. Sci.* **354**, 1195–1213.
47. Lee, S.-P., Silva, A. C., Ugurbil, K., and Kim, S.-G. (1999). Diffusion-weighted spin-echo fMRI at 9.4T: microvascular/tissue contribution to BOLD signal changes. *Magn. Reson. Med.* **42**, 919–928.
48. Movshon, J. A., Thompson, I. D., and Tolhurst, D. J. (1978). Spatial and temporal contrast sensitivity of neurons in areas 17 and 18 of the cat's visual cortex. *J. Physiol.* **283**, 101–120.
49. Otsuka, R., and Hassler, R. (1962). Ueber Aufbau und Gliederung der corticalen Sehsphaere bei der Katze. *Archiv fuer Psychiatrie und Zeitschrift f. d. Ges. Neurologie* **203**, 212–234.
50. Mansfield, P. (1977). Multi-planar image formation using NMR spin echoes. *J. Physiol. C* **10**, L55–L58.
51. Turner, R., Le Bihan, D., Moonen, C. T., Despres, D., and Frank, J. (1991). Echo-planar time course MRI of cat brain oxygenation changes. *Magn. Reson. Med.* **22**, 159–166.
52. Bandettini, P. A., Jesmanowicz, A., Wong, E. C., and Hyde, J. S. (1993). Processing strategies for time-course data sets in functional MRI of the human brain. *Magn. Reson. Med.* **30**, 161–173.
53. Albus, K. (1975). A quantitative study of the projection area of the central and the paracentral visual field in area 17 of the cat II. The spatial organization of the orientation domains. *Exp. Brain Res.* **24**, 181–202.
54. Loewel, S., and Singer, W. (1990). Tangential intracortical pathways and the development of iso-orientation bands in cat striate cortex. *Dev. Brain Res.* **56**, 99–115.
55. Kim, D.-S., and Bonhoeffer, T. (1994). Reverse occlusion leads to a precise restoration of orientation preference maps in visual cortex. *Nature* **370**, 370–372.
56. Jezzard, P., Rauschecker, J. P., and Malonek, D. (1997). An in vivo model for functional MRI in cat visual cortex. *Magn. Reson. Med.* **38**, 699–705.
57. Gonzalez, R. C., and Woods, R. E. (1993). *Digital image processing*. New York, Addison-Wesley.
58. Roland, P. E., Eriksson, L., Stone-Elander, S., and Widen, L. (1987). Does mental activity change the oxidative metabolism of the brain? *J. Neurosci.* **7**, 2373–2389.
59. Fox, P. T., and Raichle, M. E. (1986). Focal physiological uncoupling of cerebral blood flow and oxidative metabolism during somatosensory stimulation in human subjects. *Proc. Natl. Acad. Sci. U.S.A.* **83**, 1140–1144.
60. Turner, R., and Grinvald, A. (1994). Direct visualization of patterns of deoxyhemoglobin and reoxygenation in monkey cortical vasculature during functional brain activation. *Proc. 2nd Soc. Magn. Reson. Med.*, 430.
61. Vanzetta, I., and Grinvald, A. (1999). Increased cortical oxidative metabolism due to sensory stimulation: implications for functional brain imaging. *Science* **286**, 1555–1558.
62. Shmuel, A., and Grinvald, A. (1996). Functional organization for direction of motion and its relationship to orientation maps in cat area 18. *J. Neurosci.* **16**, 6945–6964.
63. Maldonado, P. E., Goedecke, I., Gray, C. M., and Bonhoeffer, T. (1997). Orientation selectivity in pinwheel centers in cat visual cortex. *Science* **276**, 1551–1555.
64. Crair, M. C., Gillespie, D. C., and Stryker, M. P. (1998). The role of visual experience in the development of columns in cat visual cortex. *Science* **279**, 566–570.